PROCEEDINGS OF SCIENCE

Searches for Point-like Sources of Cosmic Neutrinos with 15 Years of ANTARES Data

Sergio Alves Garre[a] **and Giulia Illuminati**[b,*] **on behalf of the ANTARES Collaboration**

[a] *Intituto de Física Corpuscular, IFIC (CSIC - Universitat de València)*
Calle Catedrático José Beltrán 2, 46980 Paterna, Valencia, España
[b] *INFN - Sezione di Bologna,*
Viale Berti-Pichat 6/2, 40127 Bologna, Italy

E-mail: Sergio.Alves@ific.uv.es, giulia.illuminati@bo.infn.it

The high-energy neutrino telescope ANTARES was a water-Cherenkov detector anchored to the deep bottom of the Mediterranean Sea. It took its last data in February 2022, after 15 years of operation, and had as main goal the identification of neutrinos from astrophysical sources. Given its advantageous view of the Southern Sky, in particular for neutrino energies below 100 TeV, and its excellent angular resolution, the telescope represented a powerful tool to search for the presence of point-like sources, especially of Galactic origin. The ANTARES Collaboration has consistently updated the results of the search for cosmic point-like neutrino sources using all the available data at the time. With the detector now decommissioned, the final update to this analysis using the complete dataset collected between early 2007 and early 2022 is presented and discussed in this contribution.

38th International Cosmic Ray Conference (ICRC2023)
26 July - 3 August, 2023
Nagoya, Japan

*Speaker

PoS(ICRC2023)1128

1. Introduction

The ANTARES neutrino telescope [1], decommissioned on February 2022 after 15 years of operation, consisted of a three-dimensional array of 885 photomultiplier tubes distributed along 12 lines separately horizontally 70 m. Each line hosted 25 storeys equipped with three photomultiplier tubes each one shielded by a presure-resistant glass sphere. The vertical distance between storeys was 14.5 m. Anchored at a depth of 2500 meters below the Mediterranean Sea's surface and located 40 km off the coast of Toulon, France, this unique setup offered clear visibility of neutrinos coming from the Southern Sky and the Galactic Centre. Immersed in seawater and nestled in the Northern Hemisphere, ANTARES boasted an exceptional angular resolution, rendering it an excellent tool for pinpointing cosmic neutrinos sources, particularly of Galactic origin.

Within this contribution, the findings of several searches for point-like sources utilising ANTARES data collected over its complete lifetime of 15 years are presented. This contribution not only updates the previous analysis [2] by adding two more years of data, but it uses an improved dataset obtained by means of refined calibrations, recovered data from previous years of operation, and incorporates simulated ν_τ events. Moreover, an update of the energy estimator for tracks which takes into account the time evolution of the detector over the whole data-taking period has been included.

The ANTARES neutrino telescope is sensitive to two different morphologies of light emission in water: tracks and showers. The former are produced by muons crossing the water at relativistic speeds, coming from the charged current interactions of ν_μ with the medium. The latter originate mainly from ν_e and ν_τ interacting through charged current, and neutral current neutrino interactions for all three flavours. This final data set comprises 11029 tracks and 239 showers recorded during 4541 days of effective livetime between January 29, 2007 and February 13, 2022. The selection criteria is based on maximising the model discovery potential of a neutrino flux with a spectrum proportional to E^{-2}, as described in [3].

2. Search method

Due to the unavoidable atmospheric neutrino background, the analysis method is based on searching for spatial clustering events from any direction of the sky. The estimated energy of the events is also used, as cosmic neutrinos are predicted to be produced with a harder spectrum than the atmospheric background (neutrinos and muons). For this task, and unbinned maximum likelihood, defined as follows, is used:

$$\log \mathcal{L} = \sum_{j}^{N_{\text{sam}}} \sum_{i}^{N_j} \log \left[\frac{\mu_{\text{sig}}^j}{N_j} \mathcal{S}_i^j + (1 - \frac{\mu_{\text{sig}}^j}{N_j}) \mathcal{B}_i^j \right] \tag{1}$$

where the sum over j represents all considered samples, tracks and showers in this work. Then, for each j-th sample, $\mathcal{S}_i^j$ and $\mathcal{B}_i^j$ are the values of the signal and background probability density functions (PDFs) of the i-th event, and N^j is the total number of events observed in the j-th sample. The signal and background PDFs are given by the product of a directional and an energy term. The same definition of the PDFs employed in the previous analyses [2, 3] is used. The

likelihood of Equation (1) is maximised in search for the best value of the total fitted signal events: $\mu_{\rm sig} = \mu_{\rm sig}^{\rm track} + \mu_{\rm sig}^{\rm shower}$. The significance of each inspected sky location is determined by a test statistic (TS) computed as:

$$Q = \log \mathcal{L}(\mu_{\rm sig}^j = \mu_{\rm max}^j) - \log \mathcal{L}(\mu_{\rm sig}^j = 0), \tag{2}$$

that is, the difference between the log-likelihood for the best fit of the free parameter $\mu_{\rm sig}$ and the value of the log-likelihood on the background-only hypothesis. The distributions of the TS are built from pseudo-experiments (PEs), which consist of fake samples composed only of background-like events which maintain the properties of the declination, right ascension, and energy distributions of real data. The significance of the observed $Q_{\rm data}$ from the true dataset is obtained computing the p-value in the only-background TS distribution.

3. Searches and Results

Two different searches for cosmic neutrinos are carried out: a scan over the full ANTARES sky map looking for clusters of events, and a search from very specific directions determined by the location of interesting sources which are candidates to be neutrino emitters.

3.1 Full-sky search

For this type of search, the complete celestial sky below 40° in declination (limit of the ANTARES visibility) is divided in a grid of $\sim (0.11^\circ \times 0.11^\circ)$ pixels covering equal areas in solid angle using the HEALPix[1] tool [4, 5]. Each direction, determined by the coordinates of the centre of the pixel, is studied using the likelihood of Equation (1), and the $Q_{\rm pixel}$ obtained from this direction is compared to its corresponding $Q_{\rm bkg}$ distribution at the same declination. With this procedure the ANTARES sky map of neutrinos is transformed into the map of pre-trial p-values of Figure 1, where the colour code indicates the magnitude of the p-value found on each direction.

The pre-trial p-values must be corrected by the number of performed trials (directions studied) during the analysis. To do so, the same analysis is repeated over many PEs composed of only background-like events. For each PE, the lowest p-value found on the sky is saved to build the distribution of the lowest p-values . Then, the post-trial p-value is computed as the significance of the pre-trial p-value from real data in this lowest p-values distribution.

The location of the sky with highest significance is spotted at equatorial coordinates $(\alpha, \delta) = (200.5^\circ, 17.7^\circ)$, with a pre-trial p-value of 3×10^{-5} (post-trial p-value of 1.1%), corresponding to 4.0σ (1.2σ) in the one-sided convention. Figure 2a shows the pre-trial p-values sky map in a $10^\circ \times 10^\circ$ square centred at the location of the hotspot, while Figure 2b depicts the ANTARES events located close to the same sky direction. The closest astrophysical object is the radio source J1318+1807, located at a distance of 1.0° from the hotspot. Other sources within 2.0° are J1315+1736 (1.5°) and J1328+1744 (1.7°). The location of the second most significant spot is found in the Southern Sky at $(\alpha, \delta) = (183.2^\circ, -16.1^\circ)$ with 3.7σ pre-trial significance.

[1] http://healpix.sourceforge.net

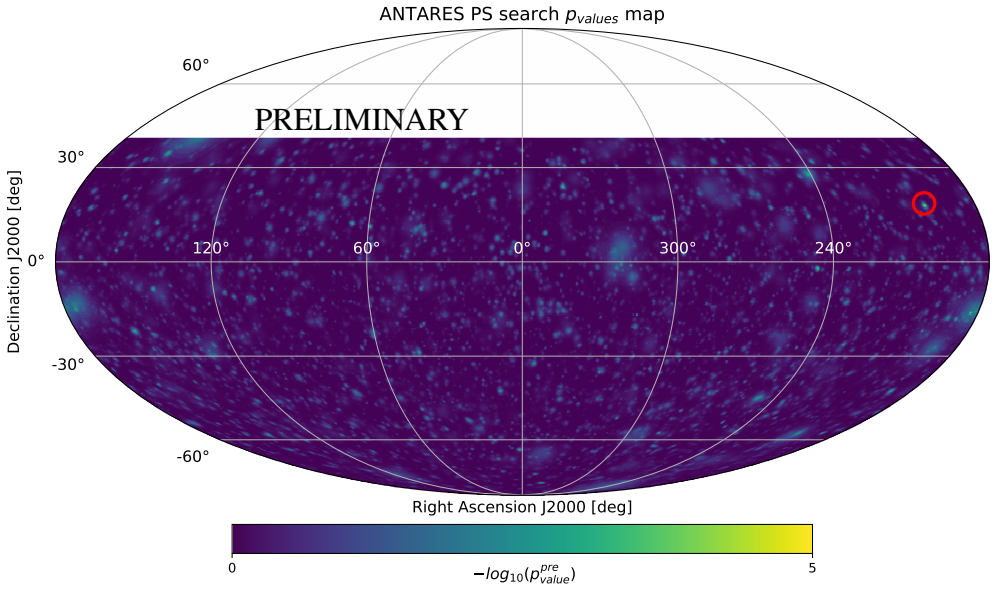

Figure 1: Sky map in equatorial coordinates of pre-trial p-values for a point-like source of the ANTARES visible sky. The red circle indicates the spot on the sky with the highest significance.

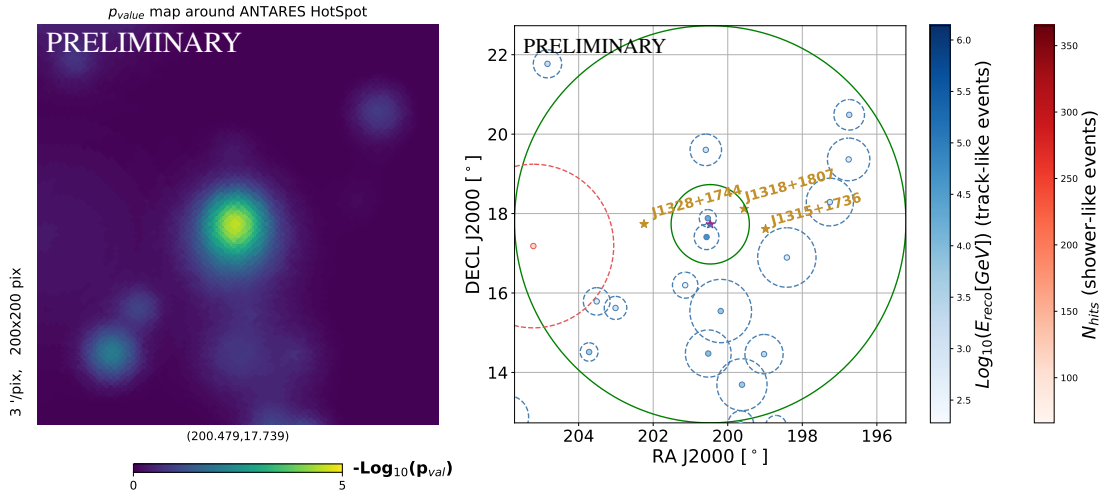

(a) **(b)**

Figure 2: **(a)**: Pre-trial p-value map around the location of the full-sky hotspot. **(b)**: Distribution of the ANTARES events close to the full-sky hotspot in the (α, δ) = (200.5°, 17.7°) coordinates. The inner (outer) solid green line depicts the one (five) degree distance from the position of the source location. The red points denote shower-like events, whereas the blue points indicate track-like events. The dashed circles around the events indicate the angular error estimate. Different tones of red and blue correspond to the values assumed by the energy estimators as shown in the legend. The location and names of the three astrophysical sources located closer than 2.0° from the hotspot are reported in golden.

3.2 Candidate-list search

In the candidate-list search, a set of directions determined by the position of known promising sources is investigated in search of cosmic neutrino signal. The studied list in this work is an update of the previous one analysed in [2] with the following modifications:

- Seven new Galactic sources from the TeVCat catalogue [6] have been added.
- Eleven new sources listed in the first LHAASO catalogue [7] have been added.
- All HAWC sources updated to the third catalogue [8].
- Potential neutrino-emitting radio blazars from a previous KM3NeT analysis [9] have been added.
- Two sources that are significant from a previous ANTARES analysis [10]: MG3 J225517+2409 and 3C403.
- The direction of the hottest spot in the IceCube Southern Sky from [11].

The list of the 163 analysed candidates, together with the obtained results at each location, is reported in Table 1. The search results in blazar MG3 J225517+2409 being the most significant one of the list. A pre-trial p-value of 3.34×10^{-4} is found, corresponding to 3.4σ in the one-sided convention, and translating into a 0.054 post-trial significance of 1.7σ. Figure 3a shows the pre-trial p-value sky map in a $10^\circ \times 10^\circ$ square centred at the location $(\alpha, \delta) = (343.8^\circ, 24.2^\circ)$, while Figure 3b depicts the ANTARES events located close to the same sky direction. The 90% C.L. limits on the one-flavour neutrino flux normalisation, Φ_0, are shown in Figure 4 as a function of the declination for the 163 investigated candidates. The neutrino flux has been parameterised as $\Phi_\nu = \Phi_0 \left(\frac{E_\nu}{1\,\mathrm{GeV}}\right)^{-2}$.

4. Conclusions

The results of searches for point-like sources using events detected by the ANTARES telescope during 15 years of data taking have been presented. The searches include a scan over the whole ANTARES visible sky and an investigation of 163 astrophysical candidates. No significant evidence of cosmic neutrino sources has been found. The full-sky hotspot $(\alpha, \delta) = (200.5^\circ, 17.7^\circ)$ has a pre-trial p-value of 3×10^{-5} (4.0σ), corresponding to 1.1% post-trial p-value. The sources investigated in the candidate-list search showing highest pre-trial significance above 2σ are: MG3 J225517+2409 (3.4σ), 3C403 (3.4σ), J0242+1101 (2.6σ), J2136+0041 (2.4σ), TXS 0506+056 (2.4σ), J0609-1542 (2.3σ) and the Galactic Centre (2σ).

Acknowledgement

The authors of this work acknowledge the financial support of grant PRE2019-087798 funded by MCIN/AEI/10.13039/501100011033 and by ESF Investing in your future, and by grant of the Generalitat Valenciana, Pla GenT: references CIDEGENT/2018/034 & 2020/049.

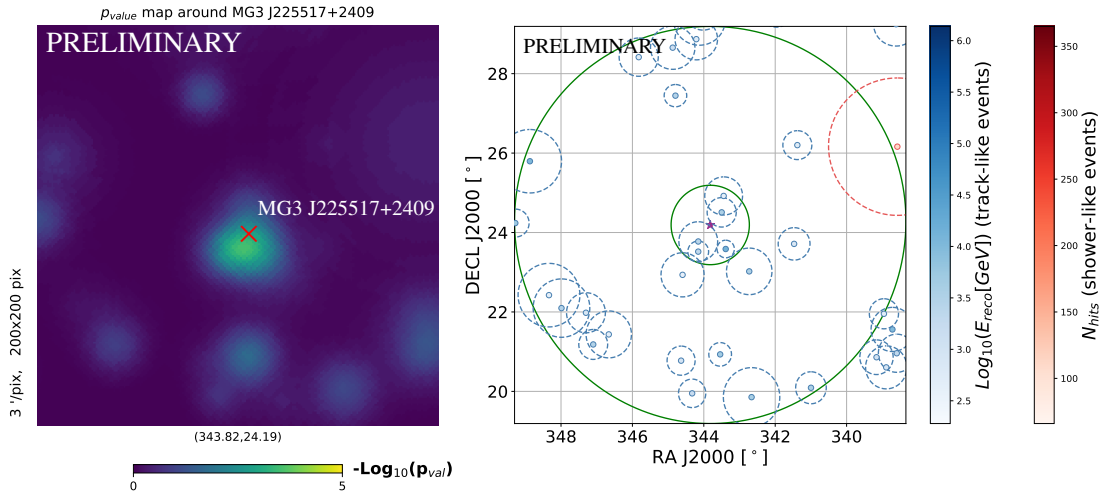

(a) **(b)**

Figure 3: (a): Pre-trial p-value map around the location of the most significant source MG3 J225517+2409. **(b)**: Distribution of the ANTARES events close to MG3 J225517+2409 in the (α, δ) = (343.8°, 24.2°) coordinates. Refer to the caption of Figure 2b for a description of the map.

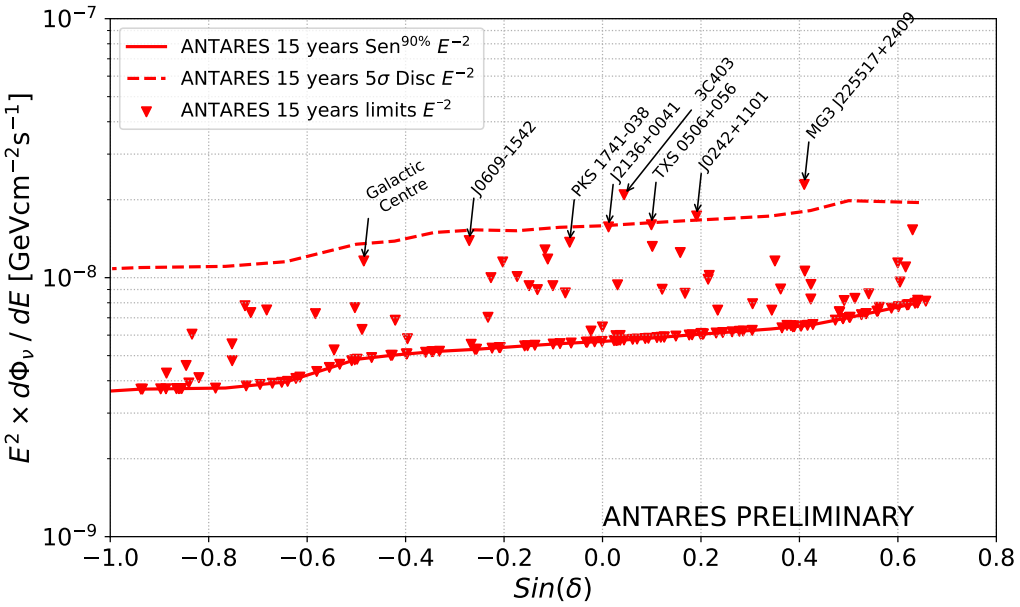

Figure 4: 90% C.L. upper limits (triangles) on the one-flavour neutrino flux normalisation for the investigated astrophysical candidates as a function of the source declination. A $E^{-2.0}$ spectrum has been assumed. The arrows point to the the upper limits corresponding to the sources for which a pre-trial significance of over 2σ has been obtained. The solid (dashed) line shows the 90% C.L. median sensitivity (50% 5σ discovery flux) of the analysis.

Table 1: List of analysed astrophysical objects. Reported are the source's name, declination δ, right ascension α, best-fit number of signal events $\hat{\mu}_{\rm sig}$, pre-trial p-value and 90% C.L. upper limits on the flux normalisation factor for a $E^{-2.0}$ spectrum, $\Phi_0^{90\%\rm C.L.}$ (in units of 10^{-8} GeVcm^{-2}s^{-1}). Sources for which a pre-trial significance of over 2σ has been obtained are highlighted in bold. Dashes (–) in the fitted number of source events and pre-trial p-value indicate sources with null fitted signal.

Name	$\delta[^\circ]$	$\alpha[^\circ]$	$\hat{\mu}_{\rm sig}$	p-value	$\Phi_0^{90\%\rm C.L.}$	Name	$\delta[^\circ]$	$\alpha[^\circ]$	$\hat{\mu}_{\rm sig}$	p-value	$\Phi_0^{90\%\rm C.L.}$
LMCN N132D	-69.5	81.2	–	–	0.37	RGBJ0152+017	1.79	28.17	–	–	0.57
LHA 120-N-157B	-69.16	84.43	–	–	0.37	J1229+0203	2.05	187.5	–	–	0.60
PSRB1259-63	-63.83	195.70	–	–	0.37	HESS J1858+020	2.06	284.57	–	–	0.57
RCW86	-62.48	220.68	–	–	0.37	**3C403**	**2.51**	**298.07**	**3.21**	**0.000337**	**2.09**
HESS J1507-622	-62.34	226.72	–	–	0.43	1LHAASO J1858+0330	3.51	284.59	–	–	0.57
ESO 139-G12	-59.94	264.41	–	–	0.37	CGCG 420-015	4.03	73.38	–	–	0.58
SNR G318.2+00.1	-59.46	224.42	–	–	0.37	SS433	4.98	287.96	–	–	0.58
MSH 15-52	-59.16	228.53	–	–	0.37	J0433+0521	5.35	68.30	–	–	0.58
HESS J1503-582	-58.74	226.46	–	–	0.37	**TXS 0506+056**	**5.7**	**77.35**	**2.5**	**0.0083**	**1.6**
HESS J1023-575	-57.76	155.83	–	–	0.46	HESS J0632+057	5.81	98.24	1.66	0.036	1.32
CirX-1	-57.17	230.17	–	–	0.37	LHAASO J1908+0621	6.35	287.05	–	–	0.58
IC$_{hotspot}$ South	-56.5	350.2	0.4	0.19	0.61	1LHAASO J1902+0648	6.8	285.58	–	–	0.59
SNR G327.1-01.1	-55.08	238.65	–	–	0.41	PKS 2145+067	6.96	327.02	0.29	0.21	0.92
HESSJ1614-518	-51.82	243.58	–	–	0.37	B1030-074	7.19	158.39	–	–	5.9
PKS 2005-489	-48.82	302.37	0.25	0.25	0.55	1LHAASO J906+0712	7.2	286.56	–	–	0.59
GX339-4	-48.79	255.70	–	–	0.48	3HWC J1914+118	8.57	286.79	–	–	0.59
HESS J1641-463	-46.30	250.26	2.26	0.067	0.78	W 498	9.09	287.78	1.00	0.052	1.25
RX J0852.0-4622	-46.37	133.00	–	–	0.38	OT 081	9.65	267.89	0.09	0.72	0.87
Vela X	-45.60	128.75	1.9	0.094	0.73	HESS J1921+101	10.15	288.21	–	–	0.6
PKS0537-441	-44.08	84.71	–	–	0.39	PKS 1502+106	10.49	226.1	–	–	0.6
CentaurusA	-43.02	201.36	1.05	0.085	0.75	**J0242+1101**	**11.02**	**40.6**	**4.43**	**0.00526**	**1.73**
PKS1424-418	-42.10	216.98	–	–	0.38	1LHAASO J1959+1129u	11.49	299.82	–	–	0.6
1ES2322-409	-40.66	351.20	–	–	0.38	RBS 0723	11.56	131.8	–	–	0.61
RXJ1713.7-3946	-39.75	258.25	–	–	0.40	3HWC J1914+118	11.72	288.68	–	–	0.6
CTB 37A	-38.52	258.56	–	–	0.40	J2232+1143	11.73	338.15	–	–	0.61
PKS0426-380	-37.93	67.17	–	–	0.40	J0121+1149	11.83	20.42	–	–	0.61
PKS1454-354	-35.67	224.36	1.46	0.12	0.73	J1230+1223	12.39	187.71	0.48	0.173	0.98
PKS0625-35	-35.49	96.78	–	–	0.40	J0750+1231	12.52	117.72	0.91	0.151	1.02
TXS1714-336	-33.70	259.40	–	–	0.40	PKS 1413+135	13.35	214.03	–	–	0.61
SwiftJ1656.3-3302	-33.04	254.07	–	–	0.53	J0530+1331	13.53	82.74	–	–	0.75
PKS0548-322	-32.27	87.67	–	–	0.40	W 51	14.14	290.75	–	–	0.61
H2356-309	-30.63	359.78	–	–	0.40	VER J0648+152	15.27	102.2	–	–	0.62
PKS2155-304	-30.22	329.72	–	–	0.40	J2253+1608	16.15	343.49	–	–	0.62
HESSJ1741-302	-30.20	265.25	1.2	0.095	0.77	PKS 0235+164	16.17	39.66	–	–	0.62
PKS1622-297	-29.90	246.50	–	–	0.48	PKS 0735+178	17.71	114.53	–	–	0.62
J1924-2914	-29.24	291.21	–	–	0.63	LHAASO J1929+1745	17.75	292.25	–	–	0.79
Galactic Centre	**-29.01**	**266.43**	**2.01**	**0.024**	**1.16**	J0854+2006	20.11	133.70	–	–	0.75
J2258-2758	-27.97	344.52	–	–	0.48	RGB J2243+203	20.5	340.98	0.82	0.109	1.16
J1625-2527	-25.46	246.45	–	–	0.50	VER J0521+211	21.21	80.40	–	–	0.90
NGC 253	-25.29	11.8	–	–	0.50	4C+21.35	21.38	186.23	–	–	0.64
Terzan5	-24.90	266.95	–	–	0.69	Crab	22.01	83.63	–	–	0.65
1ES1101-232	-23.49	165.91	–	–	0.51	IC 443	22.5	94.21	–	–	0.65
J0457-2324	-23.24	270.43	–	–	0.51	S20109+22	22.74	18.02	–	–	0.65
W28	-23.34	270.43	–	–	0.58	B1422+231	22.93	216.76	–	–	0.65
J1833-210A	-21.06	278.42	–	–	0.52	3HWC J1940+237	23.77	295.05	–	–	0.65
J0836-2016	-20.28	129.16	–	–	0.52	PKS 1424+240	23.8	21.76	–	–	0.65
J1911-2006	-20.12	287.79	–	–	0.52	**MG3 J225517+2409**	**24.19**	**343.82**	**4.39**	**0.00034**	**2.29**
eHWCJ1809-193	-19.34	272.46	–	–	0.53	3HWC J1950+242	24.26	297.69	–	–	0.66
J0609-1542	**-20.12**	**287.79**	**1.23**	**0.015**	**1.39**	MS1221.8+2452	24.614	186.1	–	–	0.65
SNR G015.4+00.1	-15.47	274.52	–	–	0.55	PKS 1441+25	25.03	220.99	–	–	0.83
j2158-1501	-15.02	329.53	–	–	0.52	1ES0647+250	25.05	102.69	–	–	0.65
LS5039	-14.83	276.56	–	–	0.52	S31227+25	25.3	187.56	–	–	0.66
LHAASOJ1825-1326	-13.45	276.45	–	–	0.70	W Comae	28.23	185.38	–	–	0.69
QSO1730-130	-13.10	263.30	1.41	0.104	1.00	LHAASO J1956+2864u	28.75	299.78	–	–	0.74
J1337-1257	-12.96	204.42	–	–	0.53	J0237+2848	28.8	39.47	–	–	0.74
J2246-1206	-12.11	241-58	–	–	0.53	TON0599	29.24	179.88	–	–	0.69
1ES0347-121	-11.99	57.35	–	–	0.53	1LHAASO J1219+2915	29.25	184.98	–	–	0.69
PKS0727-11	-11.70	112.58	1.52	0.051	1.15	3HWC J1951+2915	29.4	297.99	–	–	0.82
HESSJ1828-099	-9.99	277.24	0.87	0.11	1.01	1ES1215+303	30.1	184.45	–	–	0.70
J1512-0905	-9.10	228.21	–	–	0.55	1ES1218+304	30.19	185.36	–	–	0.70
HESSJ1834-087	-8.76	278.69	–	–	0.55	HESS J1746-308	30.84	266.57	–	–	0.83
J0607-0834	-8.58	-92	0.61	0.152	0.93	B21811+31	31.74	273.4	–	-	0.72
PKS1406-076	-7.90	212.20	–	–	0.55	J1310+3220	32.25	197.62	–	–	0.73
QSO2022-077	-7.60	306.40	0.59	0.17	0.89	B21420+32	32.39	215.63	–	–	0.72
RS Ophiuchi	-6.71	267.55	1.67	0.027	1.28	1LHAASO J2002+3244u	32.74	300.64	–	–	0.86
J0006m0623	-6.39	1.56	1.57	0.047	1.18	1LHAASO J2028+3352	33.88	307.21	–	–	0.74

Continuation of Table 1

Name	$\delta[^\circ]$	$\alpha[^\circ]$	$\hat{\mu}_{\rm sig}$	p-value	$\Phi_0^{90\%\text{C.L.}}$	Name	$\delta[^\circ]$	$\alpha[^\circ]$	$\hat{\mu}_{\rm sig}$	p-value	$\Phi_0^{90\%\text{C.L.}}$
3C279	-5.79	194.05	0.88	0.152	0.93	3HWC J2006+340	34.0	301.73	–	–	0.74
LHAASO J1839-0545	-5.75	279.95	–	–	0.55	J1613+3412	34.21	243.42	–	–	0.86
J2225-0457	-4.95	336.45	–	–	0.56	S30218+35	35.94	35.27	–	–	0.76
PKS 1741-038	**-3.38**	**266**	**2.71**	**0.021**	**1.37**	LHAASO J2018+3651	36.85	304.75	–	–	1.14
LHAASO J1843-0338	-3.65	280.75	–	–	0.56	1LHAASO J2027+3657	36.95	306.88	–	–	0.77
HESS J1848-018	-1.89	282.12	–	–	0.56	J2015+3710	37.18	303.87	–	–	0.96
J0339-0416	-1.78	54.88	–	–	0.56	Milagro Diffuse	38	305	0.45	0.195	1.1
J0423-0120	-1.34	65.82	–	–	0.62	Mkn 421	38.21	166.11	–	–	0.78
J0725-0054	-0.92	111.46	–	–	0.56	B32247+381	38.43	342.53	–	–	0.78
LHAASOJ1849-0003	-0.05	282.35	–	–	0.56	J0927+3902	39.04	141.76	0.98	0.043	1.53
NGC1068	-0.01	40.67	–	–	0.65	NGC 4151	39.41	182.63	–	–	0.80
J2136+0041	**0.70**	**324.16**	**2.82**	**0.0079**	**1.57**	Mkn 501	39.76	253.47	–	–	0.80
3HWC J1852+013	1.34	283.05	–	–	0.57	J1642+3948	39.81	250.75	–	–	0.82
J1058+0133	1.57	164.62	–	–	0.60	J0555+3948	39.81	88.88	–	–	0.80
J0108+0135	1.58	17.16	–	–	0.57	LHAASO J2032+4102	41.05	308.05	–	–	0.81
PKS 0736+017	1.79	28.17	–	–	0.57						

References

[1] ANTARES collaboration, *ANTARES: the first undersea neutrino telescope*, *Nucl. Instrum. Meth. A* **656** (2011) 11 [1104.1607].

[2] G. Illuminati, *Searches for point-like sources of cosmic neutrinos with 13 years of antares data*, in *Proceedings of ICRC21*, 2021.

[3] A. Albert, M. André , M. Anghinolfi, G. Anton, M. Ardid, J.-J. Aubert et al., *First all-flavor neutrino pointlike source search with the ANTARES neutrino telescope*, *Physical Review D* **96** (2017) .

[4] A. Zonca, L. Singer, D. Lenz, M. Reinecke, C. Rosset, E. Hivon et al., *healpy: equal area pixelization and spherical harmonics transforms for data on the sphere in python*, *Journal of Open Source Software* **4** (2019) 1298.

[5] K.M. Górski, E. Hivon, A.J. Banday, B.D. Wandelt, F.K. Hansen, M. Reinecke et al., *HEALPix: A Framework for High-Resolution Discretization and Fast Analysis of Data Distributed on the Sphere*, *ApJ* **622** (2005) 759 [arXiv:astro-ph/0409513].

[6] "Tevcat cataloge." http://tevcat.uchicago.edu/.

[7] Z. Cao, F. Aharonian, Q. An, Axikegu, Y.X. Bai, Y.W. Bao et al., *The first lhaaso catalog of gamma-ray sources*, 2023.

[8] A. Albert, R. Alfaro, C. Alvarez, J.R.A. Camacho, J.C. Arteaga-Velá zquez, K.P. Arunbabu et al., *3hwc: The third HAWC catalog of very-high-energy gamma-ray sources*, *The Astrophysical Journal* **905** (2020) 76.

[9] R. Muller, *Search for cosmic neutrino point sources and extended sources with 6 lines of KM3NeT/ARCA*, July, 2022. 10.5281/zenodo.6805394.

[10] A. Albert, M. André , M. Anghinolfi, G. Anton, M. Ardid, J.-J. Aubert et al., *ANTARES search for point sources of neutrinos using astrophysical catalogs: A likelihood analysis*, *The Astrophysical Journal* **911** (2021) 48.

[11] M. Aartsen, M. Ackermann, J. Adams, J. Aguilar, M. Ahlers, M. Ahrens et al., *Time-integrated neutrino source searches with 10 years of IceCube data*, *Physical Review Letters* **124** (2020) .